Measurement of electronic structure from high harmonic generation in non-adiabatically aligned polyatomic molecules

2008 New J. Phys. 10 025008

(http://iopscience.iop.org/1367-2630/10/2/025008)

New Journal of Physics
The open-access journal for physics

Measurement of electronic structure from high harmonic generation in non-adiabatically aligned polyatomic molecules

N Kajumba[1,7], R Torres[1], Jonathan G Underwood[2], J S Robinson[1], S Baker[1], J W G Tisch[1], R de Nalda[3], W A Bryan[4,8], R Velotta[5], C Altucci[5], I Procino[2], I C E Turcu[4] and J P Marangos[1,6]

[1] Blackett Laboratory, Imperial College London, London SW7 2BW, UK
[2] Department of Physics and Astronomy, University College London, Gower Street, London WC1E 6BT, UK
[3] Instituto de Química-Física Rocasolano, CSIC, 28006 Madrid, Spain
[4] Central Laser Facility, CCLRC Rutherford Appleton Laboratory, Chilton, Didcot, Oxon OX11 0QX, UK
[5] CNISM and Dipartimento di Scienze Fisiche, Universitàdi Napoli 'Federico II', Napoli, Italy
E-mail: j.marangos@imperial.ac.uk

New Journal of Physics **10** (2008) 025008 (17pp)
Received 7 September 2007
Published 29 February 2008
Online at http://www.njp.org/
doi:10.1088/1367-2630/10/2/025008

Abstract. We have explored the use of laser driven high-order harmonic generation to probe the electronic structure and symmetry of conjugated polyatomic molecular systems. We have investigated non-adiabatically aligned samples of linear symmetric top, nonlinear symmetric top and asymmetric top molecules, and we have observed signatures of their highest occupied molecular orbitals in the dependence of harmonic yields on the angle between the molecular axis and the polarization of the driving field. A good quantitative agreement between the measured orientation dependence of high harmonic generation and calculations employing the strong field approximation has been found. These measurements support the extension of molecular imaging techniques to larger systems.

[6] Author to whom any correspondence should be addressed.
[7] Present address: NRC Steacie Institute for Molecular Sciences, 100 Sussex Drive, Ottawa, Ontario, K1A 0R6, Canada.
[8] Present address: Department of Physics, Swansea University, Singleton Park, Swansea, SA2 8PP, UK.

Contents

1. Introduction

High-order harmonic generation (HHG) is one of the key phenomena in the interaction of high intensity infrared laser radiation with atomic or molecular gases. Its direct result, the production of coherent XUV beams and attosecond pulses, has met enormous interest within the laser science community [1]–[4]. On the other hand, the very nature of the HHG process, involving the collision of high energy electrons with their parent ions on a sub-femtosecond timescale, has opened a new path for the characterization of molecular structure with unprecedented time and spatial resolution.

High harmonic generation is usually described as a three step process: (i) an electron of the atom or molecule escapes the laser field distorted potential through the tunnel effect, (ii) the free electron oscillates in the IR field acquiring kinetic energy, and (iii) it recollides with the parent ion emitting the acquired energy as a single XUV photon [5, 6]. Tunnelling through the potential barrier restricts the ionization to occur from the outermost, least tightly bound electron; in addition, the macroscopic harmonic signal only builds up coherently from processes in which the electron recombines with the same initial states; therefore HHG is extremely sensitive to the structure of the highest energy electron orbital. Moreover, due to the high energy ($\sim$100 eV typically) of the electrons involved, i.e. short de Broglie wavelength, the sensitivity of HHG to molecular structure has a spatial resolution of less than 1 Å. For these reasons, HHG from molecules has arisen as a promising tool for the characterization of molecular structure and orbital symmetry. More importantly, as the three steps described above occur within a single laser cycle ($<$2.7 fs for 800 nm radiation), the imaging techniques based on HHG can attain ultrafast (sub-femtosecond) time resolution [7, 8], bringing measurements of orbital structures down to the natural timescale of the electron dynamics.

The practical implementation of these ideas requires the molecular sample to have a well-defined orientation in space with respect to the harmonic generating field. This requisite has become feasible in the last few years with the development of laser alignment methods [9]. Early work, using adiabatic alignment, demonstrated the sensitivity of the harmonic yield to the symmetry of the highest occupied molecular orbital (HOMO) in small molecules [10]–[12].

In that implementation of the technique the degree of molecular alignment created was relatively poor, and the harmonics were generated while the aligning field was still present thus influencing the measurements. More recent experiments have used a non-adiabatic alignment technique, this employs a laser pulse shorter than the rotational period of the molecule creating a rotational wave packet (coherent superposition of rotational states) which shows a strong alignment of the molecular axis along the laser field polarization. The rotational wave packet quickly dephases evolving freely after the interaction and, if the field free rotational eigenstates of the molecule have a regular spacing, such as in a linear or symmetric top molecule, the wave packet will rephase periodically reproducing the aligned states at regular periods of time (revivals) under field-free conditions. High-harmonic generation with a femtosecond laser pulse at a rotational revival allows for the study of the dependence of the harmonic yield upon the direction of the driving laser field polarization in the molecular frame. This has led to the first realization of tomographic reconstruction of the Dyson orbital of N_2 [13, 14] and the experimental observation of two-center interference effects [15]–[17].

These measurements suggest the possibility of using HHG to dynamically image molecular structure on the attosecond and angstrom scales. However, as the mathematical steps in structure retrieval from HHG are based upon the strong field approximation (SFA), concerns remain over (i) the use of the SFA in the interpretation of these measurements; and (ii) the scalability of this approach to larger molecular systems. The SFA neglects both the influence of the laser field upon the bound state prior to ionization, and the influence of the Coulombic potential of the ion upon the continuum electron. Furthermore, the SFA assumes a single electron response of an electron in the HOMO. Within these approximations, the continuum electron is described by a superposition of plane waves and the recombination step of HHG allows for the molecular orbital to be mapped out in momentum space [18]. Nevertheless, this model is not yet proven to be realistic for any molecule. The SFA lacks translational and gauge invariance [19]–[21] and the limitations derived from this problem are expected to be more significant for extended molecular systems.

Tomographic imaging therefore requires the observation of sufficiently high harmonic orders (and correspondingly high recollision electron momentum) to allow full characterization of the molecular orbital in momentum space. However, increasing molecular size is generally accompanied by a lowering of the ionization potential, and so lower laser intensities must be employed in order to avoid ionization saturation. This leads to a reduction in the order of observed harmonics, and a corresponding reduction in the momentum of the recollision electron. Such considerations motivate the work presented here, which tests the validity of the SFA in the analysis of HHG in laser aligned polyatomic hydrocarbon molecules.

There have been some studies devoted to HHG in large randomly oriented organic molecules [22]–[24], but quantitative studies in aligned systems have been confined to simple diatomic and triatomic linear molecules. Even in those cases, the assumption that the wavefunction can be properly described by a single electron orbital needs to be modified [14] so that it is now clear that what is retrieved via tomographic reconstruction is inevitably a signature of a multi-electron wavefunction. It is known that multi-electron processes may become more significant with increasing molecular size [25, 26] as, for example, the polarization of the ionic core by the laser field modifies the strong field processes.

The spatial alignment of larger polyatomic molecules poses a challenge as their rotational dynamics generally becomes more complicated. In contrast to linear and symmetric top molecules, the rotational energy level spacings for asymmetric tops are much less regular. This

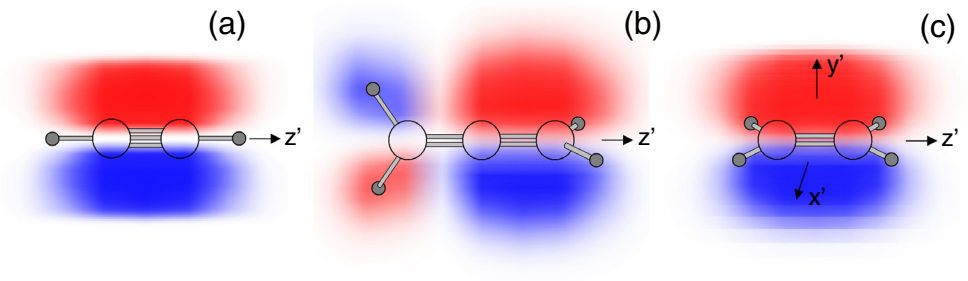

Figure 1. Representation of the HOMO in (a) acetylene, (b) allene and (c) ethylene, based upon a calculation with GAMESS-UK. In acetylene and allene only one of the two degenerate orbitals comprising the HOMO is shown. Different colors indicate different signs of the wavefunction.

complicates the rotational wave-packet evolution for asymmetric rotors and reduces alignment at revivals. The degradation of alignment worsens at elevated rotational temperatures due to the incoherent contributions of thermally populated rotational states which can lead to complete obfuscation of the rotational revival structure. This is a challenge in HHG experiments where the experiments are usually carried out in the high density region close to the throat of the molecular beam expansion where rotational cooling is compromised. Nonetheless, prompt field-free alignment is obtained after the alignment laser pulse even for highly asymmetric tops at elevated rotational temperatures as we shall show here.

The present work extends earlier studies of HHG from aligned molecules to significantly more complex systems, namely the conjugated organic molecules acetylene (HC≡CH), allene ($H_2C{=}C{=}CH_2$) and ethylene ($H_2C{=}CH_2$). These molecules have different symmetries which result in different rotational dynamics. Acetylene is a linear symmetric top ($D_{\infty h}$), allene is a prolate symmetric top (D_{2d}), and ethylene is a planar asymmetric top (D_{2h}). In acetylene, allene and ethylene the HOMO is dominated by bonding π_u orbitals between the carbon atoms (see figure 1), though the allene molecule has additional contributions to the HOMO from C–H bonds.

We have produced rotational wave packets and harmonic generation in these molecules in order to study the dependence of the harmonic yield with the angle of molecular alignment. A very short harmonic generating pulse (<15 fs) had to be used in order to prevent significant realignment of the molecules at the time of harmonic emission, and also to avoid saturation of the ionization and molecular fragmentation which would undermine the HHG [22]. In acetylene and allene good agreement with a single active electron SFA calculation was found [27]. In ethylene, though it does not show complete revivals [28], we have performed harmonic generation measurements in field-free aligned conditions using the first, post-pulse, alignment transient and again we have compared the results with a single active electron SFA calculation, taking into account the distribution of molecular orientations in the aligned sample.

This paper is organized as follows: in section 2, we present the methods employed in this work; we describe the experimental set-up for the measurements of HHG in the aligned molecular samples and the theoretical model used to simulate the experimental results, emphasizing the importance of including the distribution of molecular orientations in the simulation. Details of the calculation of molecular alignment distributions are laid out in the appendix. In section 3, we describe the harmonic spectra, rotational revivals and angular dependence of harmonic yield observed in the three molecules and discuss their comparison

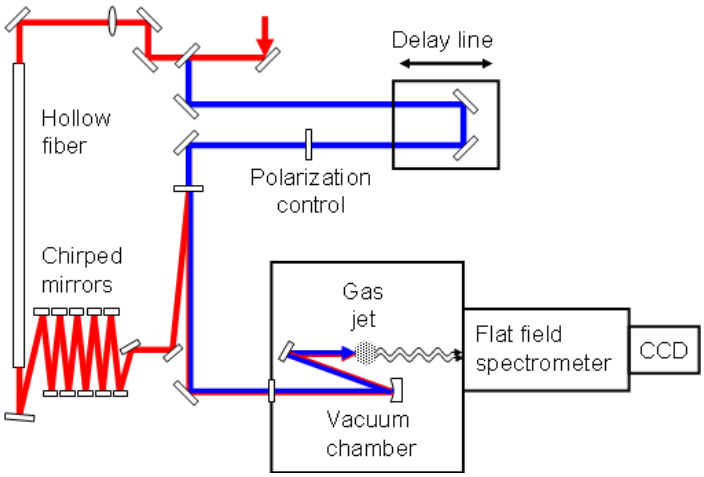

Figure 2. Schematic layout of the experiment. The blue and red lines represent the aligning and harmonic generating beams, respectively.

with simulations. In section 4, we present some conclusions and outline some issues that must be dealt with in future work.

2. Methods

2.1. Experimental set-up

The experiment was performed using the 10 Hz Astra Laser Facility at the Rutherford Appleton Laboratory, UK. This was a CPA Ti:sapphire laser system providing pulses of 35 fs after a grating compressor with energies of 16 mJ centered at 800 nm. Around 1 mJ of this energy was introduced into a differentially pumped hollow fiber filled with neon gas at 2 bars of backing pressure which was used to broaden the spectral width of the pulses in order to allow shorter pulse durations [29]. The pulses were then recollimated by a 1 m spherical mirror and compressed by a set of dielectric chirped mirrors to a duration of 10 fs measured in a single-shot second harmonic generation autocorrelator. A schematic of the experimental set-up is shown in figure 2. The experiment required two laser pulses: one to induce molecular alignment and the other to generate the harmonics, correctly synchronized with a variable delay between them. The 35 fs beam from the compressor was divided by a 80/20 beam splitter. The 80% reflected beam was used for molecular alignment and the transmitted 20% was sent to the hollow fiber for further compression and used for harmonic generation. In order to avoid stretching the pulse, all the mirrors used after the chirped mirrors were specially manufactured broadband protected silver mirrors. The two beams were recombined in a normal incidence broadband 80/20 beam splitter and propagated collinearly into the interaction chamber. The variable delay between the pulses was controlled by means of a linear stage, it was moved in steps of 25–50 fs (sufficient to resolve the revivals), and the angle Θ between the aligning and harmonic generating fields was controlled by means of a half-wave plate in the aligning beam.

The interaction chamber was maintained under a vacuum of $<10^{-5}$ mbar during the experiment. The input window was a 1 mm fused silica window with a broadband antireflection coating. The beams were focused into a pulsed gas jet with a broadband 40 cm focal length silver

coated off-axis parabolic (OAP) mirror located inside the chamber. The gas valve was mounted on a three axis manipulator controlled manually with micrometer screws. The stagnation pressure of the gases was 2 bar, and the nozzle diameter was 100 μm. The position of the laser focus relative to the nozzle made it difficult to ascertain accurately the temperature of the gas in the interaction region, nevertheless, the rotational temperature was estimated to be less than 100 K, low enough to ensure a significant degree of molecular alignment. The measured pulse durations in the interaction region were 60 fs for the aligning beam and 14 fs for the harmonic generating pulse. The lengthened duration of the alignment pulse was due to propagation through several dispersive optical components. The aligning beam had an energy of 200 μJ, giving an estimated on target intensity of $\sim 3 \times 10^{13}\,\mathrm{W\,cm^{-2}}$, which was insufficient to cause any detectable HHG. The harmonic generating beam had an energy of 300 μJ, providing an on target intensity of $\sim 1.5 \times 10^{14}\,\mathrm{W\,cm^{-2}}$.

The harmonics produced in the gas jet entered the spectrometer through a 100 μm wide entrance slit and were spatially dispersed by a flat field grating on to the detector. The detector was a 40 mm diameter, double plate imaging micro-channel plate (MCP) fitted with a phosphor screen. The image on the screen was read out by a 12-bit CCD camera and stored in a computer for later analysis. The system enabled the detection of harmonic orders from the 17th to the 59th, though the observation of harmonics from the organic molecules was limited to the 29th due to ionization saturation.

2.2. Theoretical model

The experimental measurements were simulated as follows: firstly, the harmonic spectra for different molecular orientations in the laboratory frame were calculated using the approach described by Lewenstein *et al* [30] following the assumptions of the single active electron and SFAs. We define the z-axis of the laboratory frame as the polarization direction of the linear harmonic driving field $\mathbf{E}(t)$. According to the Lewenstein model, and using the saddle-point approximation in momentum space [30], the magnitude of the time-dependent dipole moment of the system for a particular orientation, $D(t)$, can be expressed as an integral over the return time of the electron τ:

$$D(t) = \mathrm{i}\int_0^\infty \eta(\tau)E(t)d_z^*[p_{\mathrm{st}}(t,\tau) - A_z(t)]d_z[p_{\mathrm{st}}(t,\tau) - A_z(t-\tau)]\exp[-\mathrm{i}S_{\mathrm{st}}(t,\tau)]\,\mathrm{d}\tau + \mathrm{c.c.}, \tag{1}$$

where p_{st} is the momentum of the electron at the stationary points of the action, and S_{st} is the value of the stationary action. $A_z(t)$ is the z component of the vector potential of the laser field modeled as,

$$A_z(t) = -\frac{E_0}{\omega}\sin(\omega t)\cos^2\left(\frac{\pi}{2T}t\right), \tag{2}$$

where E_0 is the electric field amplitude, ω is the central frequency of the laser field and T is the pulse duration. $\eta(t)$ is a factor that accounts for the dispersion of the electronic wave packet,

$$\eta(\tau) = \left(\frac{\pi}{\epsilon + \mathrm{i}\tau/2}\right)^{3/2}, \tag{3}$$

where ϵ is a small positive constant. Finally, $d_z[p] = \langle p|z|\psi_0(\mathbf{r})\rangle$ is the transition dipole matrix element from the HOMO $\psi_0(\mathbf{r})$, expressed at a particular orientation in the laboratory frame, to

a continuum state expressed as a plane wave of momentum p. Here, the depletion of the ground state has been ignored.

The HOMO in the molecular frame $\psi_0(\mathbf{r}')$ (figure 1) were calculated as a superposition of Gaussian-like functions with the GAMESS-UK package [31] using the 321-G basis set. In all three molecules, we define the molecular z'-axis to lie along the C–C direction. In ethylene, we also define x' as an axis lying in the plane of the molecule and the y'-axis perpendicular to the molecular plane. The orientation of the molecular z'-axis in space is determined by the azimuthal and polar angles ϕ and θ, respectively. For an asymmetric top, we have to consider as well the angle χ of rotation about the molecular z' axis, which in the case of ethylene defines the orientation of the molecular plane (see appendix). The molecular and laboratory frames are connected through the rotation matrix $\tilde{\mathbf{R}}(\phi, \theta, \chi)$ [32]. Introducing $\psi_0(\mathbf{r}) = \tilde{\mathbf{R}}(\phi, \theta, \chi)\psi_0(\mathbf{r}')$ in the dipole moments of ionization and recombination, $d_z[p]$ and $d_z^*[p]$, respectively, we get the explicit dependence of equation (1) on the Euler angles ϕ, θ and χ.

As the laser field was linearly polarized, the dipole moment is independent of the angle of rotation about the polarization vector, ϕ. Furthermore, in acetylene and allene, being both symmetric top molecules, only the alignment in θ was controlled, and equation (1) must be integrated in χ. Also in these molecules the HOMO is doubly degenerate, but only one of the components needs to be considered in the calculation since any other linear combination of the two components must give the same results averaged over χ provided they are orthogonal [33]. On the other hand, ethylene can exhibit alignment in both θ and χ so we must keep the dependence on the two angles, but the HOMO of ethylene is nondegenerate.

The angle dependent harmonic spectra were calculated as:

$$S^{\mathrm{s}}(\omega; \theta) = \left|\tilde{D}^{\mathrm{s}}(\omega; \theta)\right|^2, \tag{4}$$

and

$$S^{\mathrm{a}}(\omega; \theta, \chi) = \left|\tilde{D}^{\mathrm{a}}(\omega; \theta, \chi)\right|^2, \tag{5}$$

where $\tilde{D}^{\mathrm{s}}(\omega; \theta)$ and $\tilde{D}^{\mathrm{a}}(\omega; \theta, \chi)$ are the Fourier transforms of the angle dependent dipole moments (equation (1)) for symmetric and asymmetric top molecules, respectively. The angular dependence of the amplitude and phase of each harmonic order n, for the symmetric and asymmetric molecules, was obtained as:

$$a_n^{\mathrm{s}}(\theta) = \int_{\omega_{n-1/2}}^{\omega_{n+1/2}} \left|\tilde{D}^{\mathrm{s}}(\omega; \theta)\right| \mathrm{d}\omega, \tag{6}$$

$$a_n^{\mathrm{a}}(\theta, \chi) = \int_{\omega_{n-1/2}}^{\omega_{n+1/2}} \left|\tilde{D}^{\mathrm{a}}(\omega; \theta, \chi)\right| \mathrm{d}\omega, \tag{7}$$

and

$$p_n^{\mathrm{s}}(\theta) = \arg[\tilde{D}^{\mathrm{s}}(\omega_n; \theta)], \tag{8}$$

$$p_n^{\mathrm{a}}(\theta, \chi) = \arg[\tilde{D}^{\mathrm{a}}(\omega_n; \theta, \chi)], \tag{9}$$

respectively, where ω_n is the frequency of the nth harmonic order.

In order to compare the calculations with the experimental measurements we must take into account the distribution of molecular orientations produced by the aligning pulse at time t (see appendix). As the alignment laser beam was linearly polarized, these distributions are

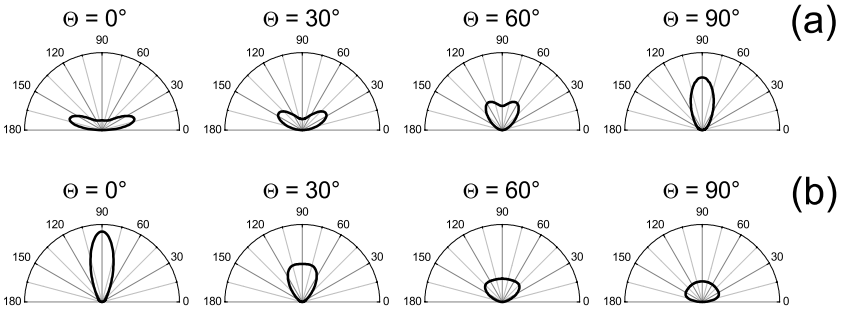

Figure 3. Variation of the characteristic polar angle distribution of aligned symmetric top molecules in the laboratory frame $\sigma^{s}(t;\Theta,\theta)$ under different aligning field angles; at the times of maximum alignment (a) or anti-alignment (b), calculated for acetylene at 50 K with an aligning pulse of 60 fs and $3\times10^{13}\,\mathrm{W\,cm^{-2}}$.

cylindrically symmetric around the aligning field axis. We define θ'' as the angle between the aligning field and the molecular axes, thus, we denote the orientation distributions of symmetric and asymmetric top molecules as $\rho^{s}(t;\theta'')$ and $\rho^{a}(t;\theta'',\chi)$, respectively. When the aligning field is rotated by an angle Θ from the harmonic generating field, the distributions seen in the frame of the latter,

$$\rho^{s}(t;\Theta,\phi,\theta)=\tilde{\mathbf{R}}(0,\Theta,0)\rho^{s}(t;\theta''), \tag{10}$$

and

$$\rho^{a}(t;\Theta,\phi,\theta,\chi)=\tilde{\mathbf{R}}(0,\Theta,0)\rho^{a}(t;\theta'',\chi), \tag{11}$$

are no longer cylindrically symmetric. We have used the rotation matrix in Θ only as the other two Euler angles for this frame transformation are zero by virtue of the co-propagation of the laser pulses.

The polar angle distributions probed by the harmonic generating field are thus obtained as:

$$\sigma^{s}(t;\Theta,\theta)=\int_{0}^{2\pi}\rho^{s}(t;\Theta,\phi,\theta)\sin(\theta)\,\mathrm{d}\phi, \tag{12}$$

and

$$\sigma^{a}(t;\Theta,\theta,\chi)=\int_{0}^{2\pi}\rho^{a}(t;\Theta,\phi,\theta,\chi)\sin(\theta)\,\mathrm{d}\phi \tag{13}$$

for every sampling angle Θ. Figure 3 shows the variation of the distributions $\sigma^{s}(t;\Theta,\theta)$ under different sampling angles when t corresponds to the time of maximum alignment or anti-alignment (planar delocalization) calculated for acetylene at 50 K with an aligning pulse of 60 fs and $3\times10^{13}\,\mathrm{W\,cm^{-2}}$. The same behavior applies for the polar angle distributions of an asymmetric top disregarding the alignment in χ. The range of angles sampled as well as the width of the distribution depend on the degree of alignment acquired in the sample, which in turn depends on the aligning field intensity and the temperature of the sample as well as the molecular properties (polarizability, anisotropy and rotational constants) [34]. In any case, the alignment and anti-alignment distributions differ notably, the latter showing a smaller variation with Θ

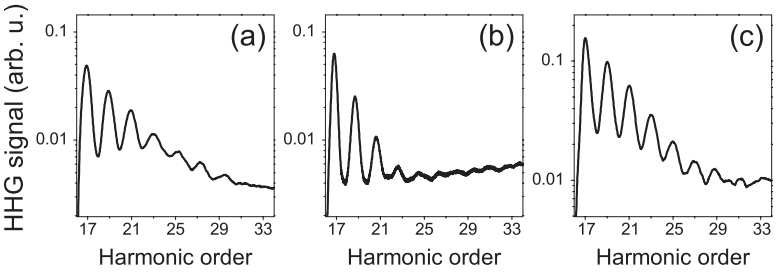

Figure 4. Harmonic spectra observed in isotropic samples of (a) acetylene, (b) allene, and (c) ethylene with a 14 fs laser pulse of $\sim 1.5 \times 10^{14}\,\mathrm{W\,cm^{-2}}$.

(therefore the harmonic yields are expected to have less dependence on Θ when measured in an anti-aligned sample).

The experimental angular dependence of the nth harmonic yield measured at a time t after the aligning pulse is:

$$S_n^{\mathrm{s}}(t;\Theta) = \left| \int_0^{\pi} a_n^{\mathrm{s}}(\theta)\,\exp[\mathrm{i}\,p_n^{\mathrm{s}}(\theta)]\,\sigma^{\mathrm{s}}(t;\Theta,\theta)\,\mathrm{d}\theta \right|^2 \tag{14}$$

for the symmetric top molecules, and

$$S_n^{\mathrm{a}}(t;\Theta) = \left| \int_0^{2\pi} \int_0^{\pi} a_n^{\mathrm{a}}(\theta,\chi)\,\exp[\mathrm{i}\,p_n^{\mathrm{a}}(\theta,\chi)]\,\sigma^{\mathrm{a}}(t;\Theta,\theta,\chi)\,\mathrm{d}\theta\,\mathrm{d}\chi \right|^2 \tag{15}$$

for the asymmetric. The calculated harmonic signals were normalized by the intensities calculated in an isotropic ensemble, S_{0n}, using in that case $\sigma^{\mathrm{s}}(\Theta,\theta) = \sin\theta/2$ and $\sigma^{\mathrm{a}}(\Theta,\theta,\chi) = \sin\theta/4\pi$ for the symmetric and asymmetric top molecules, respectively.

Due to the uncertainty in the rotational temperature of the samples the calculations have been made for three different temperatures, namely 20, 50 and 100 K. To match the measurement conditions the aligning pulse intensity used in the calculations was $3 \times 10^{13}\,\mathrm{W\,cm^{-2}}$ and the pulse duration was taken to be 60 fs. The harmonic generating pulse was assumed to have an intensity of $1.5 \times 10^{14}\,\mathrm{W\,cm^{-2}}$ and 14 fs duration.

3. Results and discussion

3.1. Harmonic spectra

High harmonic generation was observed in acetylene, allene and ethylene gases. The spectra obtained from isotropic samples are shown in figure 4. Harmonics from the 17th to the 29th order were detected in acetylene and ethylene whereas in allene the maximum order detected was the 25th. This is compatible with the lower ionization potential of allene (9.69 eV), which in acetylene is 11.40 eV and in ethylene is 10.51 eV.

Increasing the laser intensity did not increase the number of harmonics observed. This suggests that the saturation of the ionization was soon reached. A way to increase the number of harmonics would be to use a longer wavelength driving field; in this manner the ponderomotive energy could reach higher values while keeping the laser intensity low enough to prevent saturation of the ionization. This was beyond the scope of the present work as a suitable laser was not available.

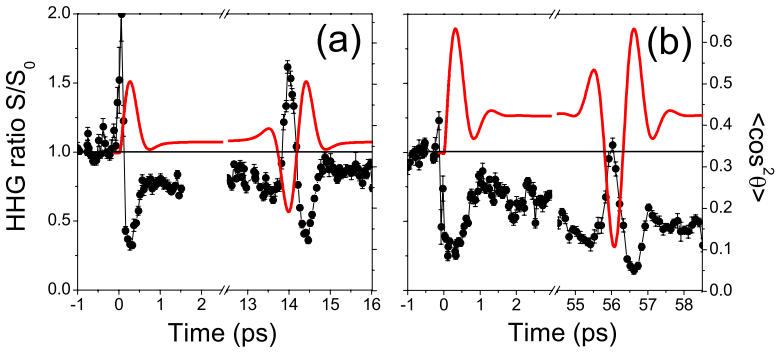

Figure 5. Ratio of harmonic intensity between aligned and isotropic samples as a function of time delay between the aligning and harmonic generating pulses for: (a) 17th harmonic in acetylene and (b) 17th harmonic in allene. The red curves show the calculated evolution of $\langle\cos^2\theta\rangle$.

3.2. Rotational revivals

In order to observe the modulation in harmonic signal caused by the alignment of the molecules, the harmonic spectra were recorded for different time delays between the aligning and driving pulses while maintaining their polarizations parallel. Spectra were also recorded in the absence of aligning field under otherwise identical conditions; when correctly calibrated, these spectra were used to extract the signal ratio between the aligned and isotropic samples. The harmonic generating beam thus probes the molecular ensemble at different instants of the alignment evolution accessed by scanning the delay through the transient rotational revivals where a rapid transition from the aligned to the anti-aligned states occurs. The degree of alignment may be represented by the expectation value $\langle\cos^2\theta\rangle$, where θ is the angle between the molecular axis (i.e. the C–C bond axis) and the aligning field polarization. The value of $\langle\cos^2\theta\rangle$ ranges from 0 for perfect anti-alignment to 1 for perfect alignment; an isotropic sample has $\langle\cos^2\theta\rangle = 1/3$.

Acetylene and allene, both being symmetric top molecules, exhibit regular rotational energy level spacings, which result in regular revivals of the molecular axis alignment after the aligning pulse [9]. The measured signal ratio for the 17th harmonic in acetylene and allene is shown in figures 5 (a) and (b), respectively. Also in figure 5, the evolution of $\langle\cos^2\theta\rangle$ calculated in a full quantum mechanical treatment is represented [35]. The harmonic signal for all detected orders showed a modulation as a function of the time delay between the aligning and harmonic generating pulses that was anti-correlated with $\langle\cos^2\theta\rangle$, indicating a suppression in the harmonic yield when the molecules are aligned with their axes parallel to the driving field polarization. Some degree of incoherent permanent alignment [36, 37] was also evidenced as a constant signal suppression between the revivals.

The temporal structure of the revivals in the asymmetric top molecule ethylene is more complicated than that of a symmetric top. As the projection of the angular momentum along the molecular axis is not conserved, states of different periodicity can be populated by the aligning field. Due to the lack of regularity in the rotational level spacings, the rotational components of the wave packet do not fully rephase and hence, the alignment is not periodic [28, 38]. Partial revivals are produced at times around 9 and 18 ps after the laser interaction [28]. The measured harmonic signal (figure 6) showed a deep modulation corresponding to the prompt alignment, immediately after the laser interaction, followed by some smaller features coincident with the

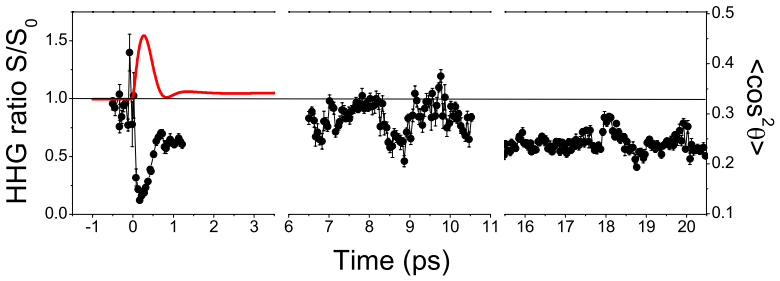

Figure 6. Ratio of harmonic intensity between aligned and isotropic samples as a function of time delay between the aligning and harmonic generating pulses for the 17th harmonic in ethylene. The red curve shows the post-pulse evolution of $\langle\cos^2\theta\rangle$ calculated classically.

expected partial revival times. The degree of alignment $\langle\cos^2\theta\rangle$ in this case was calculated classically for the post-pulse transient only [39]. As in acetylene and allene, the harmonic signal modulates in the opposite direction to $\langle\cos^2\theta\rangle$ meaning that, again, the harmonic emission is minimum when the molecules are aligned in the direction of the field.

3.3. Angular dependence of harmonic yield

The angular dependence of the harmonic yield from acetylene and allene was measured setting the delay between the aligning and driving fields at times corresponding to the maximum molecular alignment (along the laser field) or maximum anti-alignment (located preferentially in the plane perpendicular to the aligning field) in the first rotational revival. In ethylene, where no complete revivals are produced, the measurements were taken in the first alignment transient immediately after the interaction; at this time the alignment is maximum and is already field-free as the aligning pulse has just passed. The harmonic signal was then recorded as a function of the angle Θ between the aligning and driving field polarization directions.

The angular dependences of the signal ratio taken at the time of maximum alignment in acetylene ($t = 14.38$ ps), allene ($t = 56.55$ ps), and ethylene ($t = 0.2$ ps), are plotted in the top row of figures 7–9, respectively. For all harmonic orders in the three molecules, the harmonic order is suppressed when the molecules are predominantly parallel to the field, as already deduced from the revival structure, and increases with the angle Θ. In acetylene and allene, measurements could be taken as well at points of maximum anti-alignment ($t = 14.00$ and 56.00 ps, respectively). In this case, the signal ratios displayed the opposite trend with Θ to those taken at the maximum alignment, as expected (bottom row of figures 7 and 8) although with a smaller modulation, due to the less significant changes of the angular distribution with Θ (figure 3).

These results show a significant contrast between allene and the other two molecules. While in acetylene and ethylene, the maximum harmonic signal ratio is reached at $\Theta = 90^\circ$, in allene the maximum is shifted to $\Theta < 90^\circ$. This is a direct consequence of its different molecular orbital structure.

The measured angular dependence of the harmonic yields can thus be readily related to the shape of the HOMO orbitals. The signal suppression around 0° is due to the nodal plane in the orbitals, which contain the molecular axes, and the signal for larger angles increases

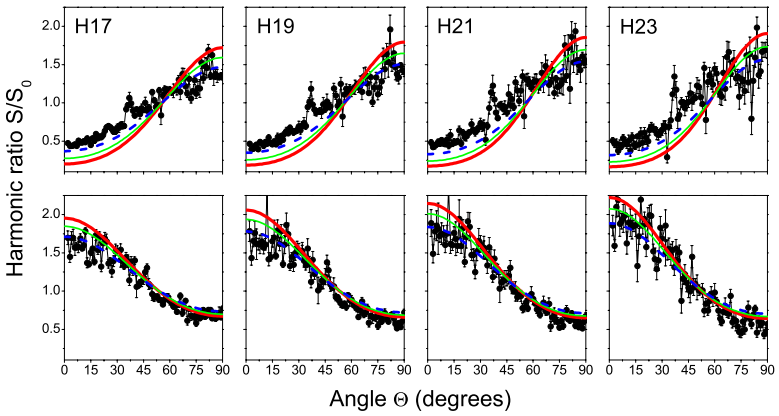

Figure 7. Harmonic ratio between aligned and isotropic samples of acetylene molecules as a function of the angle between the aligning and driving field polarizations, measured at the alignment peak ($t = 14.38$ ps) (top row) and anti-alignment peak ($t = 14.00$ ps) (bottom row). The red thick solid, green thin solid and blue dashed curves show the calculated ratio in a sample at 20, 50 and 100 K, respectively.

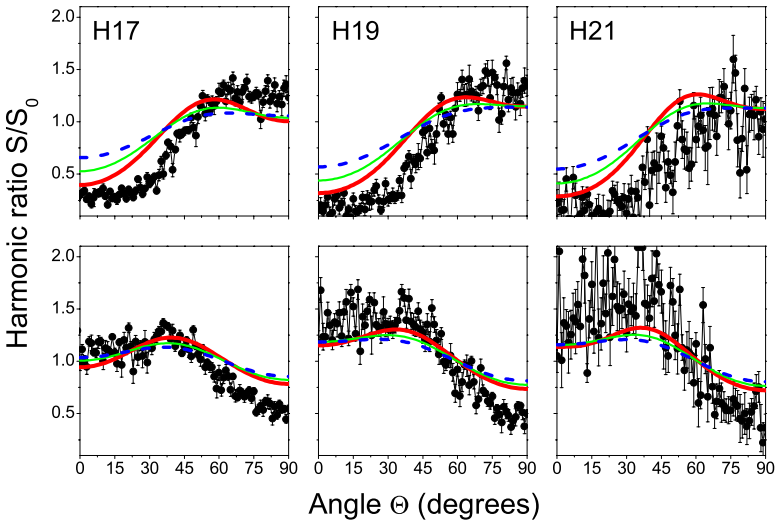

Figure 8. Harmonic ratio between aligned and isotropic samples of allene molecules as a function of the angle between the aligning and driving field polarizations, measured at the alignment peak ($t = 56.55$ ps) (top row) and anti-alignment peak ($t = 56.00$ ps) (bottom row). The red thick solid, green thin solid and blue dashed curves show the calculated ratio in a sample at 20, 50 and 100 K, respectively.

as the electron density in the direction of the field grows larger. In the case of acetylene and ethylene, the maximum occurs in the direction perpendicular to the molecular axis; this behavior is characteristic of a π_u orbital. In allene, while the general trend shows the same pattern as acetylene and ethylene in accordance with the same π_u structure that dominates the HOMO, the

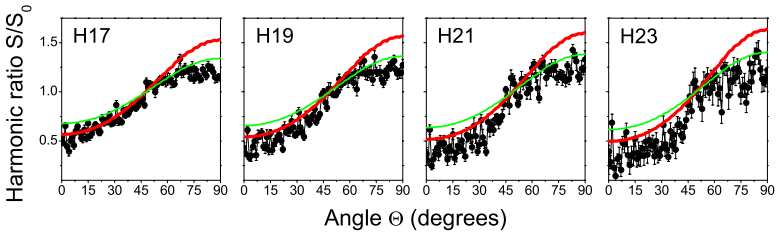

Figure 9. Harmonic ratio between aligned and isotropic samples of ethylene molecules as a function of polarization angle between aligning and driving beams, measured at the time of maximum alignment ($t = 0.20$ ps). The red thick and green thin curves show the calculated ratios in a sample at 20 and 50 K respectively.

additional electron amplitude around the hydrogen atoms causes a clear difference in the signal at large sampling angles. These results agree with the interpretation of previous measurements of HHG in N_2 and O_2 where the angular dependence has been found to be characteristic of their HOMO structure (σ_g and π_g, respectively) [40]–[42]. However, this is clear evidence that the effect of subtler structural details of the molecular orbital can be observed in the angular dependence of the harmonic signal from more complex molecules.

The theoretical simulations agree well with the observed angular dependence of the harmonic ratio both qualitatively and quantitatively. The calculated data for 20, 50 and 100 K are plotted in figures 7–9. The modulation of the calculated signal with the sampling angle Θ depends upon the degree of alignment in the molecular ensemble, as expected. In spite of the temperature uncertainty, the calculations reproduce the measured ratios and, more importantly, the subtle difference observed in allene typifying its orbital structure.

It has been demonstrated that HHG does not really map the structure of the HOMO but that of the Dyson orbital [14]. Therefore, a more accurate calculation should include antisymmetrized multi-electron wavefunctions. Moreover, when the ionization from the HOMO is strongly suppressed due to the presence of a nodal plane [43, 44], the contributions to the harmonic signal from lower lying electronic states may become comparable to that of the HOMO. However, the HOMO is usually a good approximation to the Dyson orbitals and the aim of this work is partly to show to what extent this approximation holds.

Another effect worth discussing is the well-known structural rearrangement of allene, from D_{2d} to D_{2h} symmetry, upon ionization. If this rearrangement is fast enough, it would reduce the intensity of the higher harmonics (those whose electron trajectories have spent more time in the continuum) as the overlap between the nuclear wave functions at the time of ionization and recombination (not included in equation (1)) would be smaller [7]. This effect is consistent with the reduced yield of higher harmonics in allene as compared with the other two molecules.

We also note that for ethylene, the alignment laser tends to localize the most polarizable axis (the C=C axis) towards the aligning field polarization direction ($\theta = 0$ and 180°) as for the symmetric top case. For molecules whose C=C axes lie along the polarization, no localization in χ is achieved, but for molecules lying towards $\theta = 90^\circ$, the laser field acts to localize the molecular x'-axis towards the laser field causing a localization in χ.

4. Conclusion

In summary, non-adiabatic molecular axis alignment has been produced in linear symmetric top, nonlinear symmetric top and asymmetric top molecules, acetylene, allene and ethylene, respectively, and high-order harmonics have been generated from these molecules with 14 fs laser pulses. A time dependent modulation of the harmonic signal has been observed as the ensemble undergoes the subsequent alignment revivals, or partial revivals in the case of ethylene. Measurement of the signal for different alignment angles shows behavior that contains the fingerprint of the bonding π_u structure in the HOMO of the molecules studied. Even the more complex nature of the HOMO of allene gives rise to a robust signature in the orientation dependence of the harmonic signal, normalized to the yield from an isotropic sample. Furthermore, the results in ethylene demonstrate that, in spite of its lack of complete rotational revivals, satisfactory measurements can be carried out in the first post-pulse alignment transient (immediately after the aligning pulse), considering that, even with a single linearly polarized pulse, the distribution of molecular orientations shows localization in two angles. These results have been reproduced by calculations performed in the frame of the SFA taking into account the appropriate description of the distribution of molecular orientations produced in the experiment. These findings confirm the importance of the molecular structure in the process of HHG found in previous works [12, 13, 40–42, 44], extend it to larger polyatomic molecules and demonstrate the sensitivity of HHG to details in the HOMO.

The range of harmonics explored here is insufficient to carry out a complete tomographic reconstruction of the orbitals. Nevertheless, the present measurements represent a step forward in the generalization of the HHG imaging technique to more complex molecules by showing that angular dependence measurements of HHG can be performed even in asymmetric top molecules and that the SFA can still be adequately employed to interpret the results. This also implies that, for these molecules at least, a calculation using only a single electron wavefunction is sufficient to capture the main features of the angular dependence of HHG.

Future development of this work includes using a longer wavelength driving field to increase the number of harmonics produced and perform measurements of the dependence of the harmonic signal with the ellipticity of the field to extract more information on the electron recollision process, essential for the molecular imaging technique.

Acknowledgments

We gratefully acknowledge the support of the staff of the Central Laser Facility at Rutherford Appleton Laboratory and James Lazarus from Imperial College London for technical assistance. R T also acknowledges the Spanish Department of State of Education and Universities, and the European Social Fund for financial support. The experiment time was granted by the CCLRC (experiment A2P2/05) in the Target Area One of the Astra Laser Facility. This work has been supported by EPSRC and RC UK.

Appendix A. Calculation of molecular alignment distributions

The distribution of molecular orientations must be calculated in a different way depending on whether the molecule is a linear symmetric top, nonlinear symmetric top, or asymmetric top. The polarizabilities and rotational constants used in the calculations are listed in table A.1.

A.1. Linear symmetric top—acetylene

In the case of a linear symmetric top the rotational states are labeled with the quantum numbers J and M. The rotational energies are $E_{\rm rot} = B\,J(J+1)$, where B is the rotational constant. Provided the aligning field is linearly polarized, the projection of the angular momentum on the laboratory-fixed z-axis is conserved and the aligned states can be expressed as a superposition of rotational states with different J:

$$|\psi_{J_{\rm i}M_{\rm i}}(t)\rangle = \sum_{J\geqslant|M_{\rm i}|} F_{J_{\rm i}J}(t)|JM_{\rm i}\rangle, \tag{A.1}$$

where $J_{\rm i}$ and $M_{\rm i}$ denote the quantum numbers of the initial rotational state, and $F_{J_{\rm i}J}(t)$ are the time-dependent complex coefficients of the wave packet. The eigenfunctions associated with the numbers J and M are the spherical harmonics $Y_J^M(\theta,\phi)$, so the distribution of molecular orientations after averaging $J_{\rm i}$ and $M_{\rm i}$ over a Boltzmann distribution at temperature T can be written as:

$$\rho(t;\theta) = \sum_{J_{\rm i}} w_{J_{\rm i}} \sum_{M_{\rm i}} \sum_{J} \sum_{J'} F^*_{J_{\rm i}J'}(t) F_{J_{\rm i}J}(t)\, Y_{J'}^{M_{\rm i}*}(\theta,\phi) Y_J^{M_{\rm i}}(\theta,\phi), \tag{A.2}$$

where $w_{J_{\rm i}}$ are the coefficients of the thermal distribution, which do not depend on $M_{\rm i}$, the summation in $M_{\rm i}$ extends from $-J_{\rm i}$ to $J_{\rm i}$, and the lower limit of the summations in J and J' is $|M_{\rm i}|$.

The rotational wave packets and distribution of orientations of acetylene were readily calculated following the procedure described in [35].

A.2. Nonlinear symmetric top—allene

For a nonlinear symmetric top a third quantum number, K, which characterizes the projection of the angular momentum $\mathbf{J}$ on the molecule-fixed z-axis, must be added. The rotational energies of a symmetric top are $E_{\rm rot} = B\,J(J+1) + (A-B)K^2$ for a prolate molecule, and $E_{\rm rot} = B\,J(J+1) + (C-B)K^2$ for an oblate molecule. In the interaction of the aligning field with a symmetric top molecule the value of K is conserved [45], so the rotational wave packets generated in this case are:

$$|\psi_{J_{\rm i}K_{\rm i}M_{\rm i}}(t)\rangle = \sum_{J\geqslant\max(|K_{\rm i}|,|M_{\rm i}|)} F_{J_{\rm i}K_{\rm i}J}(t)|JK_{\rm i}M_{\rm i}\rangle. \tag{A.3}$$

The eigenfunctions of the Hamiltonian for the symmetric top are

$$\langle\Omega|JKM\rangle = \sqrt{\frac{2J+1}{8\pi^2}} D^{J*}_{MK}(\phi,\theta,\chi), \tag{A.4}$$

where $D^J_{MK}(\phi,\theta,\chi)$ are the Wigner D-functions. Therefore, the thermal averaged distribution of aligned symmetric tops can be written as:

$$\rho(t;\theta) = \sum_{J_{\rm i}}\sum_{K_{\rm i}} w_{J_{\rm i}K_{\rm i}} \sum_{M_{\rm i}}\sum_{J}\sum_{J'} F^*_{J_{\rm i}K_{\rm i}J'} F_{J_{\rm i}K_{\rm i}J} \frac{\sqrt{(2J+1)(2J'+1)}}{8\pi^2} \sum_{L=|J'-J|}^{J+J'} (2L+1)(-1)^{M_{\rm i}-K_{\rm i}} \times \begin{pmatrix} J' & J & L \\ M_{\rm i} & -M_{\rm i} & 0 \end{pmatrix} \begin{pmatrix} J' & J & L \\ K_{\rm i} & -K_{\rm i} & 0 \end{pmatrix} P_{\rm L}(\cos\theta). \tag{A.5}$$

Table A.1. Molecular constants used in the calculations of molecular alignment distributions. Polarizabilities (in the molecular frame) in Å^3: α_{xx}, α_{yy} and α_{zz} and rotational constants: A, B and C in cm^{-1}.

Molecule	α_{xx}	α_{yy}	α_{zz}	A	B	C
Acetylene	2.43	2.43	5.12		1.177	
Allene	4.43	4.43	8.97	4.810	0.296	0.296
Ethylene	3.682	3.251	5.022	4.864	1.001	0.828

Note that in this case, the coefficients of the Boltzmann distribution depend on J_i and K_i. The lower limit of the summations in J and J' is the largest of either $|K_\mathrm{i}|$ or $|M_\mathrm{i}|$, and both the summations in K_i and M_i extend from $-J_\mathrm{i}$ to J_i.

The allene molecule is a prolate symmetric top, however, the rotational constant A is much larger than B (see table A.1) which results in the thermal distribution being much narrower in K than in J space, therefore the population of states with $K \neq 0$ can be neglected and the rotational dynamics of allene is well approximated by a linear rotor.

A.3. Asymmetric top—ethylene

In the interaction of the aligning field with an asymmetric top molecule like ethylene, the quantum number K, is not conserved. The creation of a coherent superposition of rotational states in K, as well as in J space results in localization of the angle χ around certain values [38]. In ethylene, the molecular plane tends to align parallel to the field vector ($\chi = \pi/2, 3\pi/2$), while full delocalization of the plane occurs when the molecular axis is perfectly aligned with the field ($\theta = 0, \pi$) [28].

As a fully quantum calculation of the alignment distribution of an asymmetric top at finite temperature is computationally very expensive, the post-pulse distribution $\rho(t; \theta, \chi)$ for $t \ll T_\mathrm{rot}$ used in this work was calculated classically [39].

References

[1] Ferray M, L'Huillier A, Li X F, Lompré L A, Mainfray G and Manus C 1988 *J. Phys. B: At. Mol. Opt. Phys.* **21** L31–5
[2] Burnett K, Reed V C and Knight P L 1993 *J. Phys. B: At. Mol. Opt. Phys.* **26** 561–98
[3] Drescher M *et al* 2001 *Science* **291** 1923–7
[4] Paul P M *et al* 2001 *Science* **292** 1689–92
[5] Krause J L, Schafer K J and Kulander K C 1992 *Phys. Rev. Lett.* **68** 3535–8
[6] Corkum P B 1993 *Phys. Rev. Lett.* **71** 1994–7
[7] Baker S *et al* 2006 *Science* **312** 424–7
[8] Le V-H, Le A-T, Xie R-H and Lin C D 2007 *Phys. Rev.* A **76** 013414
[9] Stapelfeldt H and Seideman T 2003 *Rev. Mod. Phys.* **75** 543–57
[10] Velotta R, Hay N, Mason M B, Castillejo M and Marangos J P 2001 *Phys. Rev. Lett.* **87** 183901
[11] Hay N, Velotta R, Lein M, de Nalda R, Heesel E, Castillejo M and Marangos J P 2002 *Phys. Rev.* A **65** 053805
[12] de Nalda R *et al* 2004 *Phys. Rev.* A **69** 031804
[13] Itatani J *et al* 2004 *Nature* **432** 867–71

[14] Patchkovskii S, Zhao Z, Brabec T and Villeneuve D M 2006 *Phys. Rev. Lett.* **97** 123003
[15] Lein M, Hay N, Velotta R, Marangos J P and Knight P L 2002 *Phys. Rev. Lett.* **88** 183903
[16] Kanai T, Minemoto S and Sakai H 2005 *Nature* **435** 470–4
[17] Vozzi C *et al* 2005 *Phys. Rev. Lett.* **95** 153902
[18] Torres R and Marangos J P 2007 *J. Mod. Opt.* **54** 39–54
[19] Lagmago Kamta G and Bandrauk A D 2005 *Phys. Rev.* A **71** 053407
[20] Chirilă C C and Lein M 2006 *Phys. Rev.* A **73** 023410
[21] Figueira de Morisson Faria C 2007 *Phys. Rev.* A **76** 043407
[22] Hay N *et al* 2000 *Phys. Rev.* A **62** 041803
[23] Hay N, Castillejo M, de Nalda R, Springate E, Mendham K J and Marangos J P 2000 *Phys. Rev.* A **61** 053810
[24] Altucci C *et al* 2006 *Phys. Rev.* A **73** 043411
[25] Smits M, de Lange C A, Stolow A and Rayner D M 2004 *Phys. Rev. Lett.* **93** 203402
[26] Smits M, de Lange C A, Stolow A and Rayner D M 2004 *Phys. Rev. Lett.* **93** 213003
[27] Torres R *et al* 2007 *Phys. Rev. Lett.* **98** 203007
[28] Rouzée A, Guérin S, Boudon V, Lavorel B and Faucher O 2006 *Phys. Rev.* A **73** 033418
[29] Robinson J S, Haworth C A, Teng H, Smith R A, Marangos J P and Tisch J G W 2006 *Appl. Phys.* B **85** 525–9
[30] Lewenstein M, Balcou P, Ivanov M Yu, L'Huillier A and Corkum P B 1994 *Phys. Rev.* A **49** 2117–32
[31] Schmidt M W *et al* 1993 *J. Comput. Chem.* **14** 1347–63
[32] Zare R N 1988 *Angular Momentum: Understanding Spatial Aspects in Chemistry and Physics* (New York: Wiley)
[33] Kjeldsen T K, Bisgaard C Z, Madsen L B and Stapelfeldt H 2003 *Phys. Rev.* A **68** 063407
[34] Friedrich B and Herschbach D 1995 *Phys. Rev. Lett.* **74** 4623–6
[35] Torres R, de Nalda R and Marangos J P 2005 *Phys. Rev.* A **72** 023420
[36] Rosca-Pruna F and Vrakking M J J 2002 *J. Chem. Phys.* **116** 6579–88
[37] Dooley P W *et al* 2003 *Phys. Rev.* A **68** 023406
[38] Péronne E, Poulsen M D, Bisgaard C Z and Stapelfeldt H 2003 *Phys. Rev. Lett.* **91** 043003
[39] Underwood J G Manuscript in preparation
[40] Shan B, Ghimire S and Chang Z 2004 *Phys. Rev.* A **69** 021404
[41] Zhou X X, Tong X M, Zhao Z X and Lin C D 2005 *Phys. Rev.* A **71** 061801
[42] Madsen C B and Madsen L B 2006 *Phys. Rev.* A **74** 023403
[43] Muth-Böhm J, Becker A and Faisal F H M 2000 *Phys. Rev. Lett.* **85** 2280–3
[44] Shan B, Tong X M, Zhao Z, Chang Z and Lin C D 2002 *Phys. Rev.* A **66** 061401
[45] Hamilton E *et al* 2005 *Phys. Rev.* A **72** 043402